CFSRC COLLOQUIUM

Proceedings of the Cold-Formed Steel Research Consortium Colloquium
20-22 October 2020 (cfsrc.org)

The effect of mechanical and geometric uncertainty on perforated CFS bracing members

F. Gusella[1], M. Orlando[2], K. D. Peterman[3]

Abstract

In the capacity design of cold-formed steel frames with X diagonal bracings, the ratio of overstrength to slenderness is particularly critical. The diagonal elements of these braces may be fabricated with perforations at the brace ends to satisfy design and detailing requirements for capacity protection of frames with concentric X bracings. In the paper, the influence of stochasticity in the geometrical features and mechanical properties on the overall structural response of specific cold-formed steel perforated elements is assessed. The impact of statistical variation in design parameters on the yield strength, ultimate strength, and ductility is evaluated through a Monte Carlo simulation. Variability in member geometric features was determined from current design specifications, while variability in steel mechanical properties was determined via experimental testing. Monte Carlo simulations indicate a slight reduction of yield and ultimate member resistance increasing the number of holes. A normal probability distribution function, with a skewness greater than zero, which increases with a larger number of holes, characterizes both the yield and ultimate strength histogram. The work concludes providing recommendations for designers to promote utilization of perforated braces in seismically-active areas

[1] Researcher, Department of Civil & Environmental Engineering, University of Florence, Italy, federico.gusella@unifi.it
[2] Professor, Department of Civil & Environmental Engineering, University of Florence, Italy, maurizio.orlando@unifi.it
[3] Professor, Department of Civil & Environmental Engineering, University of Massachusetts Amherst, USA, kdpeterman@umass.edu

1. Introduction

Cold-formed steel (CFS) storage pallet rack are easy to assemble, with boltless connections permitting rack geometric layout to be quickly changed according to storage needs while providing stiffness against buckling [1-12]. Storage racks are often designed to considerable heights. Thus, steel bracing systems are required for stability and seismic resistance.

Structures designed based on strength capacity limit states [13] have dissipative zones, which are expected to yield first, dissipating energy through plastic mechanisms. To achieve this in active tension diagonal concentric bracings, horizontal forces are resisted by the tension diagonals only, which are additionally subjected to axial forces and plastically deform. The force-elongation relationship of tensile diagonals is influenced by several design parameters, most notably the steel material (mechanical) properties and geometric manufacturing imperfections. The propagation of uncertainty in these parameters to the structural response of the perforated CFS members is the focus of this investigation.

A mechanical model capable of describing the monotonic non-linear response of braces is developed and validated through comparison with experimental tests [14]. This model is adopted for Monte Carlo simulation of concentric X bracings under incremental static non-linear forces. The Monte Carlo simulation of several models of CFS diagonals is then used to explore the resultant variability in yield, ultimate, and global buckling forces from uncertainty in steel material properties and geometric manufacturing tolerances, with the aim to more accurately assess the structural performance of proposed concentric bracing systems [15, 16].

1.1 Structural requirements of dissipative concentric bracing systems

Earthquake resistant structures may be designed as non-dissipative or with a dissipative structural behavior. In the latter case, the dissipative capacity may be taken into account explicitly through a non-linear analysis or implicitly through a linear elastic analysis, under a reduced elastic response spectrum scaled by the seismic behavior factor. This reduction requires specific material properties to assure that members are able to provide a plastic behavior. According to Eurocode 8 and Eurocode 3:

$f_{y,max}/(1.1\gamma_{ov}f_y) \leq 1$ (being $f_{y,max}$ the actual maximum yield strength of the structural steel in dissipative zones, γ_{ov} the material overstrength factor and f_y the specified yield strength) and $f_u/f_y \geq 1.1$ (being f_u/f_y the ratio of the specified minimum ultimate tensile strength f_u to the specified minimum yield strength f_y).

Regarding design and detailing rules for frames with concentric X bracings, diagonal members must satisfy the following rules:

$1.3<\lambda\leq 2$ and $\frac{\Omega_{i,\max}}{\Omega_{i,\min}} \leq 1.25$; limits on slenderness and overstrength, respectively. The slenderness limit $\lambda \leq 2$, with λ defined as the non-dimensional column slenderness, is required to limit the inelastic deformation in the out-of-plane buckling of the compressed brace; the limit $1.3<\lambda$ is specified to avoid overloading of columns in the pre-buckling stage of the compressed diagonal. In particular, $\lambda = \sqrt{\frac{P_{y,k}}{P_{cr}}}$ is the non-dimensional slenderness, with $P_{y,k} = A_g f_{y,k}$ the characteristic yield load and $P_{cr} = \frac{\pi^2 EJ}{L^2}$ the minimum Euler's global buckling load in which, A_g is the member gross cross-section and L and J are the effective buckling length and the moment of inertia related to the critical load P_{cr}.

The limit on overstrength ratio, $\frac{\Omega_{i,\max}}{\Omega_{i,\min}} \leq 1.25$, (where Ω_i is defined as the diagonal overstrength coefficient) allows for an homogeneous dissipative behavior of diagonals in the whole structure. $\Omega_i = N_{pl,Rd,i}/N_{Ed,i}$ is the diagonal overstrength coefficient for the i-th diagonal member, with $N_{pl,Rd,i}$ the design resistance of the i-th diagonal and $N_{Ed,i}$ the design axial force in the same i-th diagonal in the seismic design situation.

In this paper, with the aim to reduce the difference between the design applied axial force $N_{Ed,i}$ and the resistance load $N_{pl,Rd,i}$ (without reducing the member slenderness), tested diagonals have arrays of holes at one member-end. These holes reduce the member gross cross-section and therefore also its plastic design resistance ($N_{pl,Rd}$), satisfying the overstrength requirement. The hole array at only one member-end does not reduce the member critical global buckling load (P_{cr}).

2. Experimental tests

2.1 CFS diagonal bracing members

A suite of full-scale perforated CFS diagonals of concentric bracing systems have been tested at the Structures and Material Testing Laboratory of the Department of Civil and Environmental Engineering of Florence. The testing apparatus is shown in Figure 1 a). Specimens are connected at both ends to fixed base plates by three M16 bolts. Experimental specimens were designed as back-to-back channel-sections. To explore the impact of holes added to the brace, failure was forced into the brace section by over-designing the connection points. Figure 2

shows the geometric features of structural members, which are later deployed in the probabilistic analysis. Table 1 gives the cross-section shapes, the net cross-section areas A_{net}, the deterministic values for material properties (yielding stress f_y and ultimate stress f_u), the number of additional holes (denoted '# holes'), hole size and cross-section class (2nd and 3rd) according to [17]. Material properties were determined from coupon tests cut from the identical steel coil from which the braces were formed. Tests were performed in accordance with [18] and the values in Table 1 represent the mean from the three coupon tests.

Brace sections were tested in two different lengths: L1=1500 mm and L2=2000 mm. Figure 2 illustrates the hole pattern and geometry for the 1500 mm specimens. In the 2000 mm specimens, the clear span between hole patterns is 500 mm longer, while the remainder of the geometry is unchanged from the 1500 mm specimens.

S1 and S2 specimens have the same short slotted holes but differ in their number: there are four holes in S1 and six in S2. The remaining specimens (S3, S4 and S5) have the same number and shape of additional holes (three long slotted holes) but differ in Eurocode 3 cross-section class (Table 1). S3 and S4 differ in the experimental yield and ultimate strength of the steel.

Table 1: Mechanical and geometric properties of steel and structural details of specimens (L1=1500 mm and L2=2000 mm).

Test	Cross-section	A_{net} [mm^2]	f_y [N/mm^2]	f_u [N/mm^2]	# holes	Hole Type	Cl.
S1-L1	n.2 U42X30X2.5	376	400	454	4	10x18	3
S2-L1	n.2 U42X30 X2.5	376	400	454	6	10x18	3
S3-L1	n.2 U42X30 X2.5	376	400	454	3	25x18	3
S1-L2	n.2 U42X30 X2.5	376	400	454	4	10x18	3
S2-L2	n.2 U42X30 X2.5	376	400	454	6	10x18	3
S3-L2	n.2 U42X30 X2.5	376	400	454	3	25x18	3
S4-L1	n.2 U42X30 X2.5	376	403	459	3	25x18	3
S5-L1	n.2 U40X29X3.0	420	411	487	3	25x18	2

2.2 Experimental protocol and results

Monotonic testing was conducted under both tension and compression. The load rate was 0.2 mm/s. Load was applied until failure. Load was measured through a load cell mounted to the test frame, and the vertical displacement at the loaded end monitored directly by a linear variable displacement transducer. Testing procedures, instrumentations and detailed test results can be found in [14].

Monotonic tensile tests demonstrated reductions in both yield and ultimate strength of the perforated diagonals due to additional holes. The additional holes behaved like fuses, in which plasticity occurs at the weakest section, leading to failure of the specimen. Figure 1 b) shows the failure mode observed in the experimental tests: elongation and ovalization of one hole progressing to eventual net section fracture.

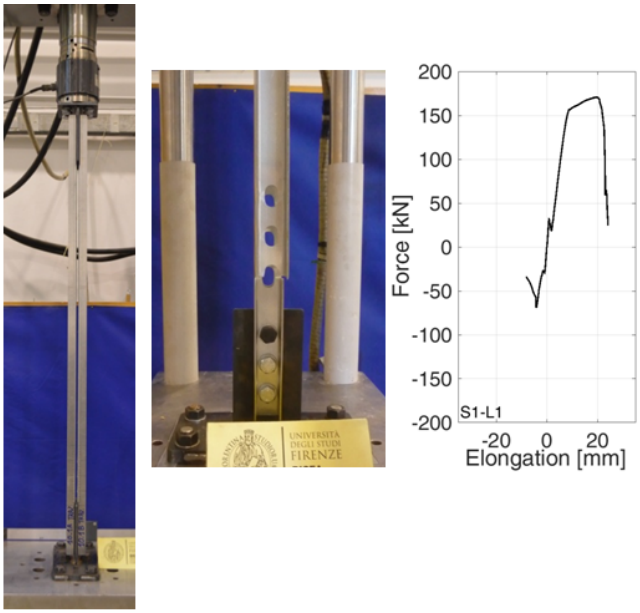

a) *b)* *c)*

Figure 1: a) Pictures of a specimen in the testing frame. b) Failure mode (S1-L1 specimen). c) Experimental force-elongation curve (S1-L1 specimen).

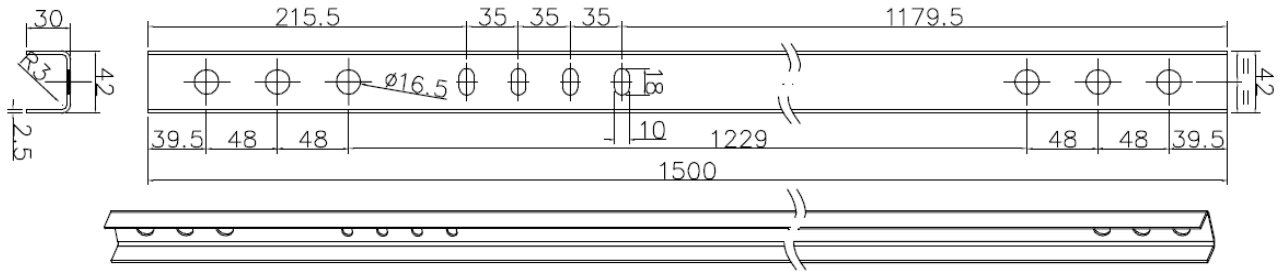

S1-L1

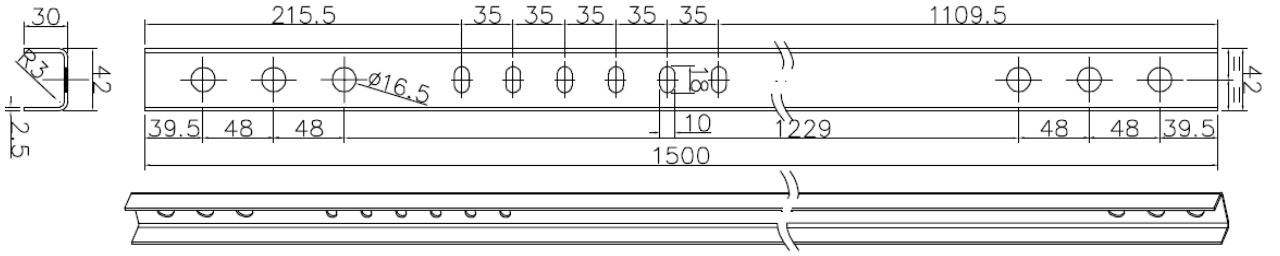

S2-L1

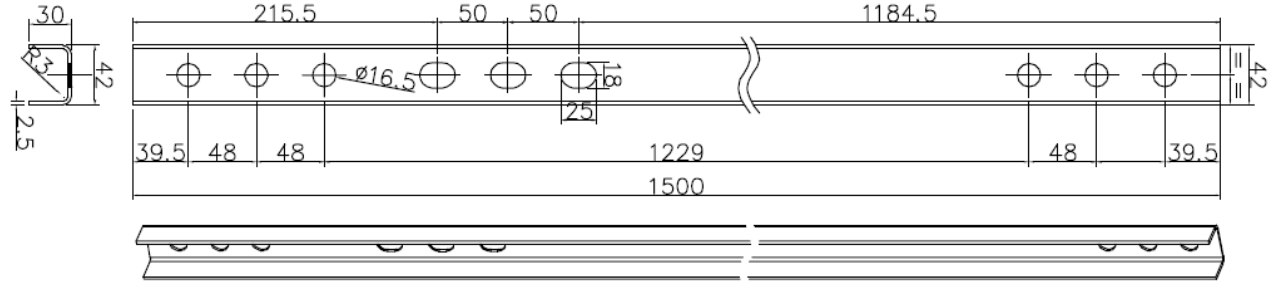

S3-L1

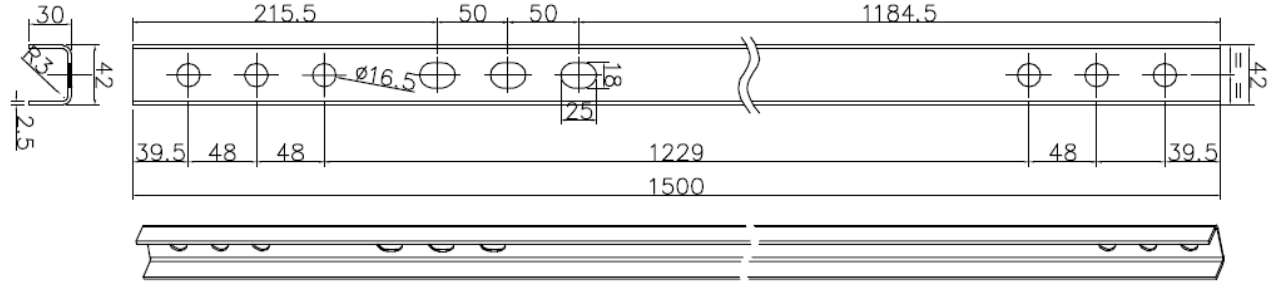

S4-L1

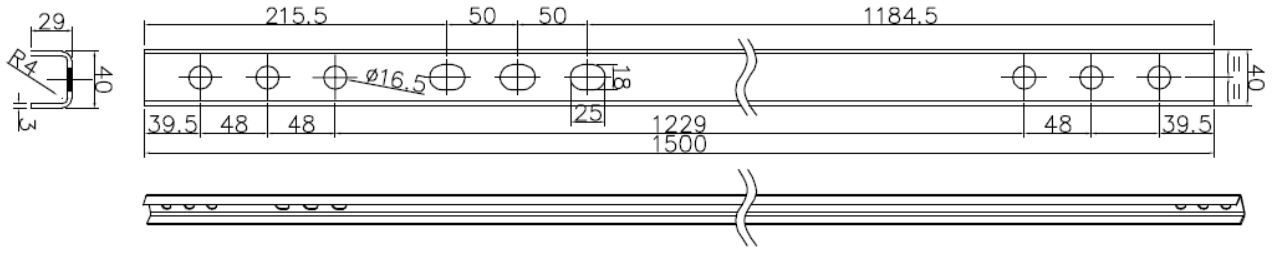

S5-L1

Figure 2: Geometry of the tested bracing specimens (L1=1500 mm). All units in mm.

3. Probabilistic analysis

3.1 Characterization of random variables

Allowable tolerances on geometric and material properties of CFS members are defined by current design specifications [19, 20].
Deterministic values for material properties (yielding stress $f_{y,Det}$ and ultimate stress $f_{u,Det}$) are reported in Table 2. The mean (μ_{MC}), coefficient of variation (V_{MC}) and probability distribution for the yield stress ($f_{y,MC}$) and ultimate stress ($f_{u,MC}$) adopted in the Monte Carlo simulations are reported in Table 2. Statistical properties of the material random variables were determined through sixty available coupon tests on different steel coils, provided by the manufacturing company which produced specimens.

Table 2: Values of yielding and ultimate strength [N/mm^2] of bracing member steel.

Deterministic Values		$f_{y,Det}$ [N/mm^2]	$f_{u,Det}$ [N/mm^2]
S1-L1	U42X30X2.5	400	454
S2-L1	U42X30X2.5	400	454
S3-L1	U42X30X2.5	400	454
S1-L2	U42X30X2.5	400	454
S2-L2	U42X30X2.5	400	454
S3-L2	U42X30X2.5	400	454
S4-L1	U42X30X2.5	403	459
S5-L1	U40X29X3.0	411	487
Probabilistic Values		$f_{y,MC}$ [N/mm^2]	$f_{u,MC}$ [N/mm^2]
U42X30X2.5	μ_{MC}	410	458
	V_{MC}	0.088	0.065
	Probability Distribution	Normal	Normal
U40X29X3.0	μ_{MC}	411	476
	V_{MC}	0.074	0.060
	Probability Distribution	Normal	Normal

S1, S2 and S3 specimens, formed from the same steel coil, have the same deterministic yield ($f_{y,Det}$) and ultimate ($f_{u,Det}$) stress. S4 and S5 are rolled from different coils and thus have slightly different material properties. Probabilistic values (the yield ($f_{y,MC}$) and ultimate ($f_{u,MC}$) stresses) for S1, S2, S3 and S4 specimens are the same, as they have identical cross-section shapes. The Young's modulus (E) was assumed normal, with V_{MC}=0.1 [21].
Member geometric parameters are assumed uniformly distributed.
The tolerances given by applicable design codes are presented in Table 3.

Table 3: Ranges of geometric parameters.

	Cross-section	Range cross-section h=height web [mm]	Range cross-section b=outside dimension [mm]	Range thickness t=[mm]
S1 S2 S3 S4	40X29X3.0	[39.25 - 40.75]	[28.2 - 29.8]	[2.8 - 3.2]
S5	42X30X2.5	[41.25 - 42.75]	[29.2 - 30.8]	[2.33 - 2.67]

The tolerance on the diameter of the additional holes (d_h=18 mm) orthogonal to the member axis was assumed ±0.5 mm in accordance with [22] for holes formed by punching. Uniformly distributed pseudorandom values are adopted for this geometric parameter.

3.2 Mechanical model

To analytically evaluate the structural response of concentric bracing systems, a mechanical model was developed.
A bilinear elastic-plastic curve describes the tensile response of member. The first branch is elastic until the yield point ($d_{y,Det}$, $T_{y,Det}$), defined by the deterministic yield elongation (1) and tensile force (2):

$$d_{y,Det} = \frac{LT_{y,Det}}{EA_{g,Det}} \quad (1)$$

$$T_{y,Det} = A_{net,Det} f_{y,Det} \quad (2)$$

where $A_{net,Det} = A_{g,Det} - t_{Det} d_h$ is the member net cross-section, $A_{g,Det}$ the member gross cross-section, t_{Det} the thickness of the specimen, d_h the diameter of additional holes orthogonal to the member axis, E the Young's modulus, L the member length and $f_{y,Det}$ the deterministic yield strength.
The second branch is linear until the ultimate point ($d_{u,Det}$, $T_{u,Det}$), defined by ultimate force (4) and displacement at ultimate force (3):

$$d_{u,Det} = d_{y,Det} + \mu \quad (3)$$

$$T_{u,Det} = A_{net,Det} f_{u,Det} \quad (4)$$

where, $\mu = 5.23\lambda - 0.50$ is the member ductility in millimeters determined from [14], $\lambda = \sqrt{\frac{T_{y,k}}{C_{cr}}}$ is the non-dimensional slenderness, with $T_{y,k} = A_{net,Det} f_{y,k}$ the nominal characteristic yield force, $f_{y,k}$ the nominal characteristic yield

strength, C_{cr} the minimum buckling load, and $f_{u,Det}$ the member ultimate strength.
In compression, behavior is assumed linear until the critical Euler buckling load (5) and corresponding elastic elongation (6):

$$C_{cr,Det} = \frac{\pi^2 EJ}{L_o^2} \quad (5)$$

$$d_{cr,Det} = \frac{LC_{cr,Det}}{EA_{g,Det}} \quad (6)$$

where, $C_{cr,Det}$ is the global buckling load, L_o is the effective buckling length, and J is the minimum moment of inertia of the specimen. This linear elastic branch is succeeded by a brittle failure until a constant value of $0.3T_{y,Det}$, in accordance with current code [13]. The simplified theoretical force-elongation curve is shown in Figure 3.

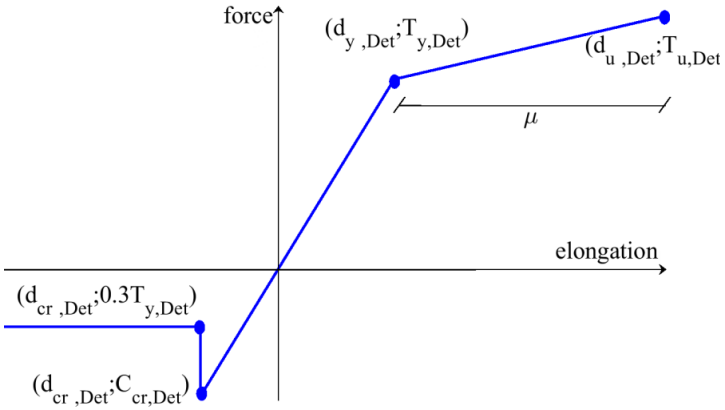

Figure 3. Force-elongation relationship of CFS perforated diagonals

3.3 Probabilistic results

To characterize the stochastic response of bracing members, 10000 samples are conducted on each diagonal in a Monte Carlo simulation.
The ratio between the mean values from simulations (MC) and the deterministic values (Det), for the yield load T_y, ultimate load T_u, buckling load C_{cr} and ductility μ, are listed in Table 4, along with the coefficient of variation (V). The ratio ≥ 1 indicates that using mean member properties on the design under-estimates the yielding load, ultimate tensile load, buckling load, and ductility; a ratio ≤ 1 indicates detrimental effects, thus a design that uses mean member properties over-estimates the mean member property.

Table 4. Ratios between Monte Carlo simulated mean values (MC) and deterministic values (Det) for yielding load (T_y), ultimate tensile load (T_u), buckling load (C_{cr}), ductility (μ). Coefficients of variation (V).

	S1-L1	S2-L1	S3-L1	S1-L2
$T_{y,MC}/T_{y,Det}$	1.02	1.02	1.02	1.02
$T_{u,MC}/T_{u,Det}$	1.01	1.00	1.00	1.01
$C_{cr,MC}/C_{cr,Det}$	1.00	1.00	1.00	1.00
μ_{MC}/μ_{Det}	1.00	1.00	1.00	0.98
VT_y	0.10	0.10	0.10	0.10
VT_u	0.08	0.08	0.08	0.08
VC_{cr}	0.12	0.12	0.12	0.12
$V\mu$	0.07	0.07	0.07	0.07

	S2-L2	S3-L2	S4-L1	S5-L1
$T_{y,MC}/T_{y,Det}$	1.02	1.02	1.01	1.00
$T_{u,MC}/T_{u,Det}$	1.00	1.01	1.00	0.97
$C_{cr,MC}/C_{cr,Det}$	1.00	1.00	1.00	1.00
μ_{MC}/μ_{Det}	0.98	0.98	0.99	0.98
VT_y	0.10	0.10	0.10	0.09
VT_u	0.08	0.08	0.08	0.07
VC_{cr}	0.12	0.12	0.12	0.12
$V\mu$	0.07	0.07	0.08	0.07

A greater coefficient of variation, V, of the yield stress compared to that of the ultimate stress reflects in $VT_y > VT_u$. Variability in the buckling load ($V \approx 0.12$) is due to the increased influence of uncertainty in geometric parameters.

3.4 Effect of additional holes

To illustrate the uncertainty propagation on the member strength due to random geometrical features of additional holes, histograms of the maximum hole diameter (d_h), yield load (T_y), ultimate load (T_u) and buckling load (C_{cr}) for S1, S2 and S3 specimens, are shown in (Figures 4-7).
The yield and ultimate load (2) (4) depend on the member net cross-section $A_{net} = A_g - d_h t$. In MC simulation the hole diameter $d_h = \max(d_{h,i})$, where $d_{h,i}$ is the hole diameter of i-th additional hole, which is affected by uncertainty.
Figure 4 demonstrates that as the number of additional holes at the member-end increases (i=3 for S3, i=4 for S1, i=6 for S2, see Figure 1), the probability of obtaining a larger hole diameter increases (mean($d_{h,S2}$) > mean($d_{h,S1}$) > mean($d_{h,S3}$)). This finding indicates that the manufacturing process itself adds to geometric imperfections.
Figure 10-11 show the comparison between histograms of the yield load (T_y), ultimate load (T_u) and buckling load (C_{cr}), obtained in the numerical simulation, and the Normal Distribution for S1, S2 and S3 specimen, in which $A_h / A_g = 20\%$ (the ratio between the hole area $A_h = d_h t$ and the member gross cross-section area A_g).

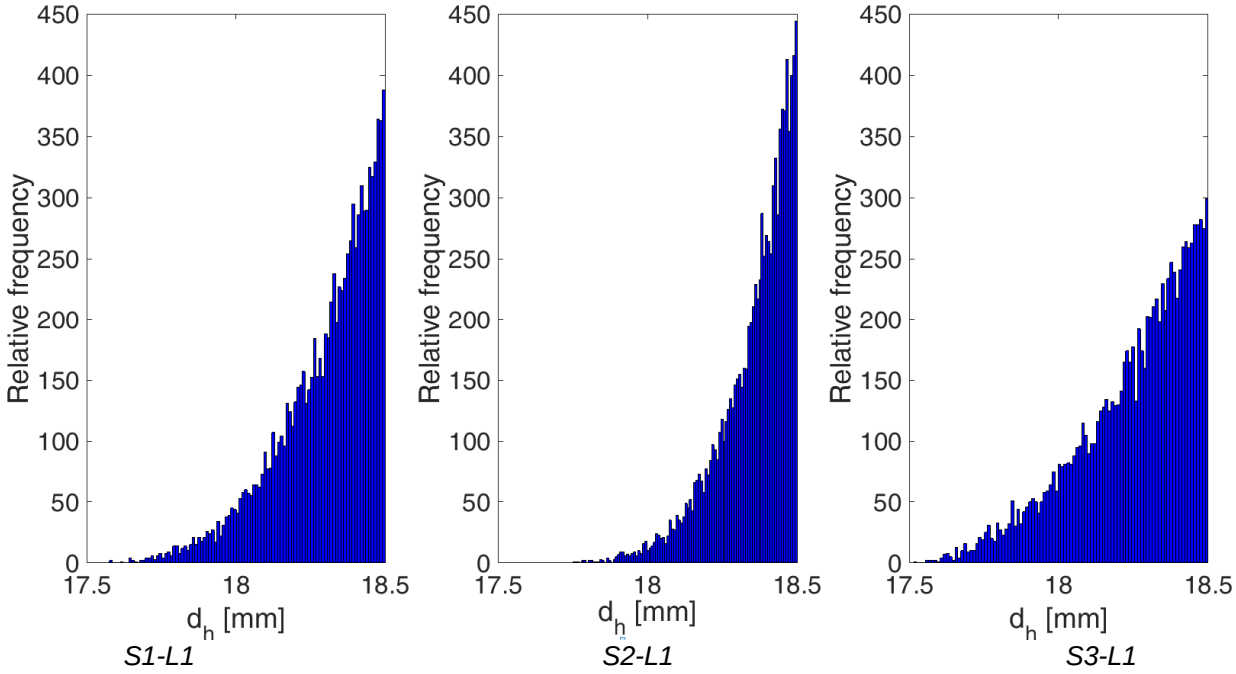

Figure 4. Histogram of the maximum hole diameter (d_h) for S1, S2 and S3 specimen, obtained in the numerical simulation.

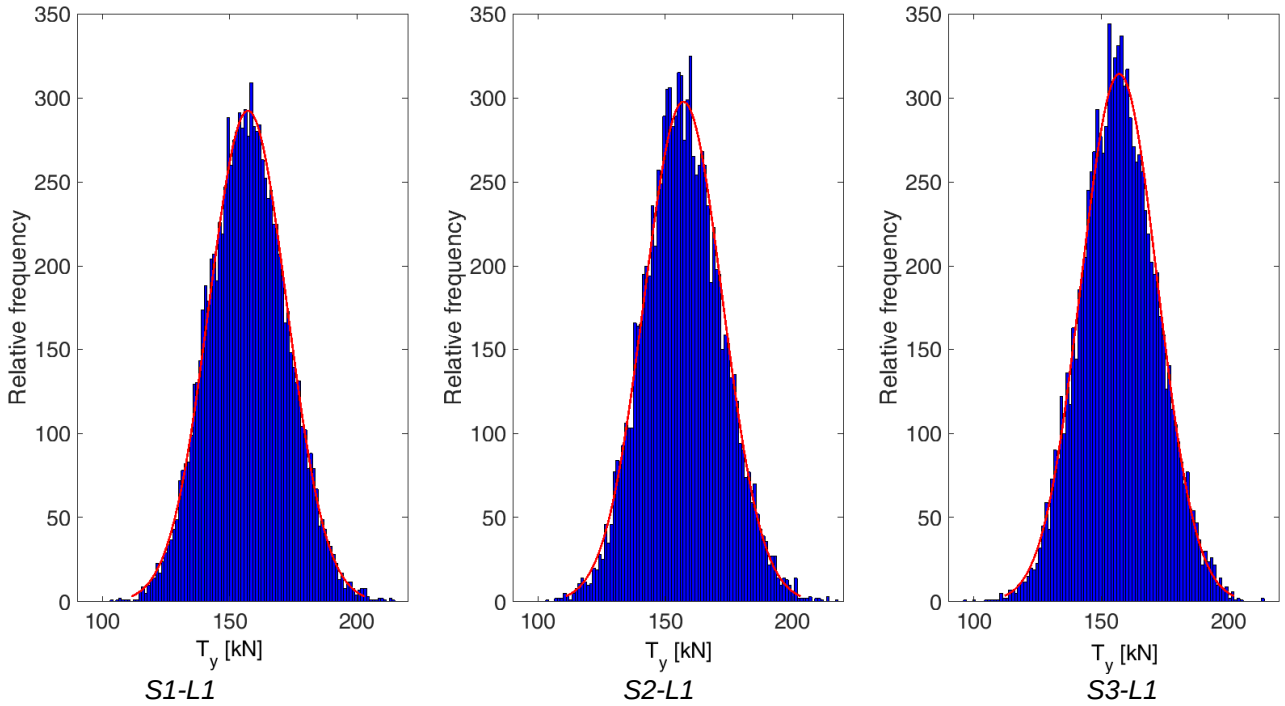

Figure 5. Comparison between histogram of the yield load (*Ty*) obtained in the numerical simulation and Normal Distribution for S1, S2 and S3 specimen.

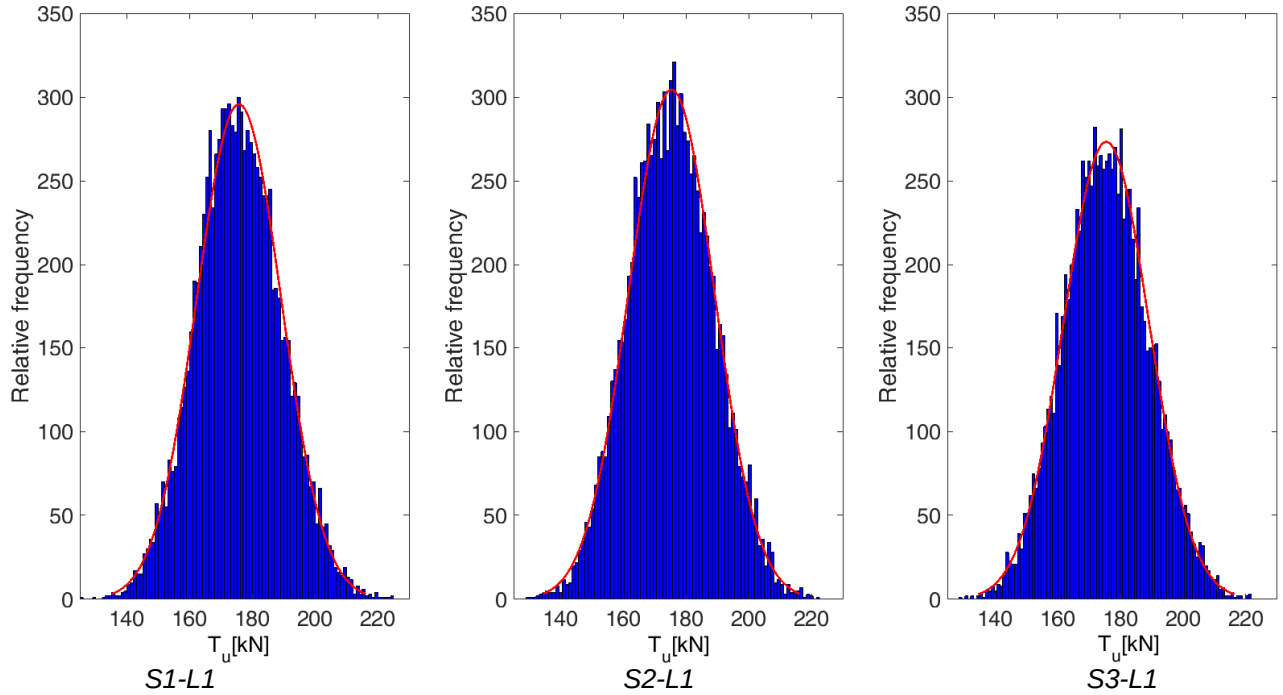

Figure 6. Comparison between histogram of the ultimate load (*Tu*) obtained in the numerical simulation and Normal Distribution for S1, S2 and S3 specimen.

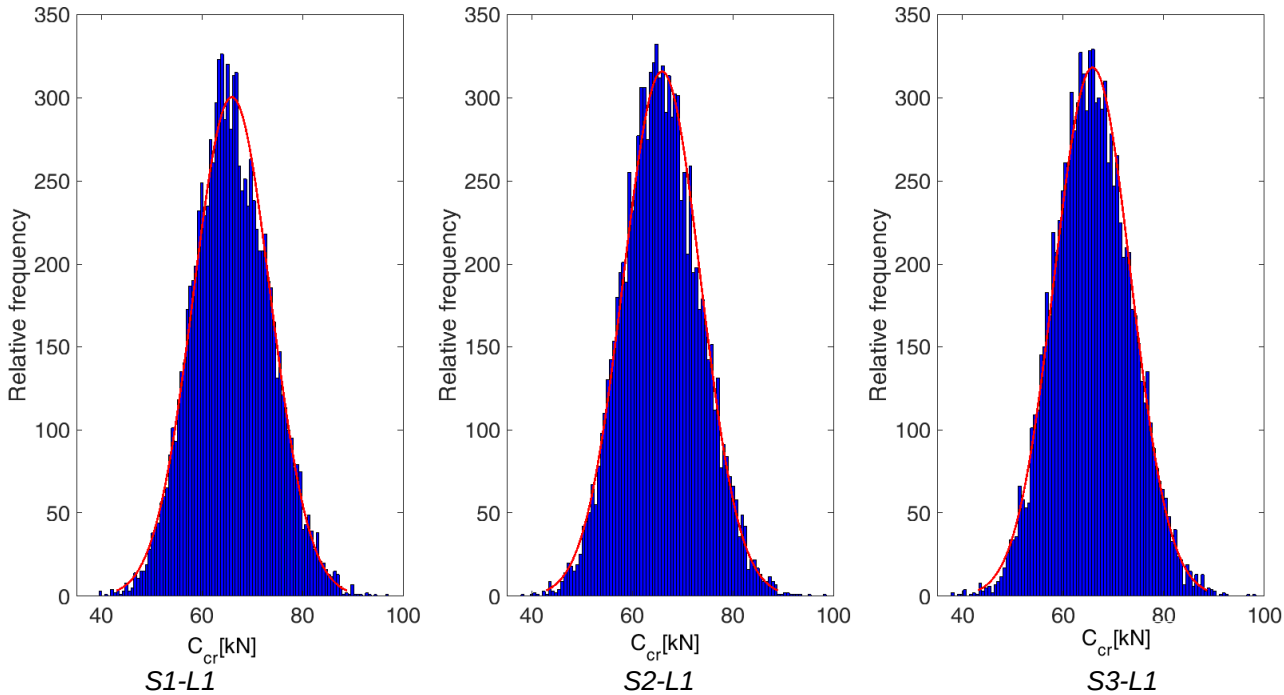

Figure 7. Comparison between histogram of the buckling load load (C_{cr}) obtained in the numerical simulation and Normal Distribution for S1, S2 and S3 specimen.

The number of holes have a slight influence on the distribution of yield load (T_y) and ultimate load (T_u). Considering members with the same nominal net cross-section and yield strength (S1, S2, S3), more holes result in a slight reduction in the mean of T_y and T_u (maximum ≈ 0.5%, for the ultimate load T_u in S2 specimen, with six

holes) and a positive skewness. The mean, coefficient of variation (V), kurtosis (K) and skewness (S) are listed in Table 5. Values of skewness (S) less than zero refer to distribution functions skewed towards the right. The buckling load C_{cr} is similar for specimens with the same gross cross-section and length (66 kN for S1-L1, S2-L1, S3-L1, S4-L1 and 35 kN for S1-L2, S2-L2, S3-L2), and is independent of the number of holes as the net section resisting buckling remains the same.

Table 5. The mean, coefficient of variation (V), skewness (S) and kurtosis (K) of maximum hole diameter (d_h), yield load (T_y), ultimate load (T_u) and buckling load (C_{cr}) obtained in Monte Carlo numerical simulations (MC).

	S1-L1	S2-L1	S3-L1	S1-L2	S2-L2	S3-L2	S4-L1	S5-L1
$d_{h,MC}$ [mm]	18.30	18.36	18.25	18.30	18.36	18.25	18.25	18.25
Vd_h	0.01	0.01	0.01	0.01	0.01	0.01	0.01	0.01
Sd_h	-1.08	-1.27	-0.90	-1.09	-1.31	-0.84	-0.87	-0.87
Kd_h	3.81	4.58	3.17	3.84	4.78	3.04	3.11	3.11
A_h/A_g	0.19	0.19	0.19	0.19	0.19	0.19	0.19	0.20
$T_{y,MC}$ [kN]	157	157	157	157	157	157	157	177
VT_y	0.10	0.10	0.10	0.10	0.10	0.10	0.10	0.09
ST_y	0.10	0.11	0.06	0.10	0.12	0.10	0.06	0.12
KT_y	2.95	3.04	2.98	2.94	3.02	2.99	2.93	2.94
$T_{u,MC}$ [kN]	176	175	176	176	175	176	176	205
VT_u	0.08	0.08	0.08	0.08	0.08	0.08	0.08	0.07
ST_u	0.09	0.09	0.06	0.09	0.10	0.09	0.17	0.14
KT_u	2.94	2.90	2.85	2.88	2.93	2.94	2.97	2.87
$C_{cr,MC}$ [kN]	66	66	66	35	35	35	66	70
SC_{cr}	0.13	0.12	0.11	0.13	0.12	0.19	0.12	0.10
VC_{cr}	0.12	0.12	0.12	0.12	0.12	0.12	0.12	0.12
KC_{cr}	2.95	2.97	2.99	2.98	3.05	3.08	2.97	3.00

A normal distribution with skewness (≈ 0.1) and kurtosis (3) is a good approximation of the tensile yield load and ultimate load histograms for cold-formed members equipped with additional holes. For the global buckling load C_{cr}, a normal distribution with skewness (≈ 0.15) and kurtosis (3) is a good approximation for its histogram.

4. Conclusions

The experimental and analytical results presented herein demonstrate that yield load, ultimate tensile load, buckling load and ductility of perforated cold-formed steel diagonals are affected by the local response of specific design parameters. This response is dependent on uncertainty in steel mechanical properties and geometric features. In order to explore the impact of these parameters, Monte Carlo simulations of several bracing members were conducted using random values to simulate the effect of the variability in the steel yield stress, steel ultimate stress and geometric features of specimens. For the Monte Carlo simulations, statistical properties of material random variables were assumed based on the results of experimental tests and the variability in geometric tolerances was assumed in accordance with current standard code requirements. The structural response of perforated members was modelled by a validated mechanical model.

Monte Carlo simulations indicate that for tested specimens, a consequence of increasing the number of same holes is a slight reduction of yield and ultimate resistance. A normal probability distribution function, with a skewness greater than zero, which increases with a larger number of holes, characterizes both the yield and ultimate strength histogram.

References

[1] K. D. Peterman, M. JJ Stehman, R. L Madsen, S. G Buonopane, N. Nakata, B. W Schafer. Experimental seismic response of a full-scale cold-formed steel-framed building. I: System-level response (2016). Journal of Structural Engineering, Volume 142, Issue 12 04016127.

[2] Bernuzzi, C., Simoncelli, M. (2016), “An advanced design procedure for the safe use of steel storage pallet racks in seismic zones”, Thin-Walled Structures, 109, 73–87.

[3] Hancock G. J. (2003), “Cold-formed steel structures”, J. Constructional Steel Research. 59 (4) 437-487.

[4] Cardoso F. S., Rasmussen K. J. R. (2016), “Finite element (FE) modelling of storage rack frames”, J. Constructional Steel Research. 126 1-14.

[5] N. Baldassino, C. Bernuzzi. Analysis and behaviour of steel storage pallet racks. Thin-Walled Structures 37 (2000) 277 – 304.

[6] M.H.R. Godley, R.G. Beale, X. Feng. Analysis and design of down-aisle pallet rack structures. Computers and Structures 77 (2000) 391-401.

[7] Gusella, F., Orlando M., Spinelli P., Pinching in Steel Rack Joints: Numerical Modelling and Effects on Structural Response. International Journal of Steel Structures (2019), 19,1, 131-146.

[8] C. Bernuzzi, C. A. Castiglioni. Experimental analysis on the cyclic behavior of beam-to-column joints in steel storage pallet racks. Thin-Walled Structures 39 (2001) 841–859.

[9] Xianzhong Zhao, Tuo Wang, Yiyi Chen, K.S. Sivakumaranc. Flexural behavior of steel storage rack beam to-upright connections. Journal of Constructional Steel Research 99 (2014) 161–175.

[10] Gusella, F., Lavacchini, G., Orlando, M., (2018), “Monotonic and cyclic tests on beam-column joints of industrial pallet racks.” Journal of Constructional Steel Research, 140, 92–107.

[11] Gusella, F., Orlando M., Thiele, K., (2018). “Evaluation of rack connection mechanical properties by means of

the Component Method". Journal of Constructional Steel Research 149, 207–224.
[12] Paolo Foraboschi P. Lateral load-carrying capacity of steel columns with fixed-roller end supports. Journal of Building Engineering, 26, 2019, 100879.
[13] Eurocode 8 – Design of structures for earthquake resistance – Part. 1: General rules, seismic actions and rules for buildings. EN 1998-1:2004.
[14] Gusella F., Lavacchini G., Orlando M., Spinelli P. (2019) "Axial response of cold-formed steel bracing members with holes". Journal of Constructional Steel Research 161, 70-85.
[15] Bian, G., Chatterjee, A., Buonopane, S.G., Arwade, S.R., Moen, C.D., Schafer, B.W., (2017), "Reliability of cold-formed steel framed shear walls as impacted by variability in fastener response". Engineering Structures 142 84–97.
[16] B.H. Smith, S.R. Arwade, B.W. Schafer, C.D. Moen. Design component and system reliability in low-rise cold formed steel framed commercial building. Engineering Structures, 127 (2016) 434-446.
[17] Eurocode 3 - Design of steel structures- Part. 1-1: General rules and rules for buildings. EN 1993-1-1, 2005.
[18] International Standard ISO 6892-1:2009. Metallic materials – Tensile testing Part1: Method of test at room temperature.
[19.] EN 10346 Continuously hot-dip coated steel flat products. Technical delivery conditions.
[20] EN 10162 Cold rolled steel sections - Technical delivery conditions – Dimensional and cross-sectional tolerances.
[21] Atua, K., Assakkaf, I. A., and Ayyub, B. M., 1996. "Statistical Characteristics of Strength and Load Random Variables of Ship Structures," Probabilistic Mechanics and Structural Reliability, Proceeding of the Seventh Specialty Conference, Worcester Polytechnic Institute, Worcester, Massachusetts.
[22] UNI EN 1090-2:2008. Execution of steel structures and aluminium structures, Part 2: Technical requirements for steel structures